Ion-collision experiments with slow, very highly charged ions extracted from an electron-beam ion trap

D. Schneider, D. DeWitt, M. W. Clark, R. Schuch,* C. L. Cocke,† R. Schmieder,‡
K. J. Reed, M. H. Chen, R. E. Marrs, M. Levine, and R. Fortner
Lawrence Livermore National Laboratory, University of California, Livermore, California 94550
(Received 25 April 1990; revised manuscript received 31 August 1990)

Highly charged Ar (up to 18+), Xe (up to 48+), and U (up to 71+) ions produced through electron-impact ionization and excitation in an electron-beam ion trap have efficiently been extracted from the trap, and mass and charge analyzed. Charge-state distributions for Ar and Xe ions following electron-impact ionization and excitation have been measured. Relative yields for the production of Ar^{16+} and Xe^{44+} ions have been deduced as a function of electron-beam energies. Ar K and Xe L x-ray emission following Ar^{17+}, Ar^{18+} and Xe^{44+}, Xe^{45+} and Xe^{48+} ion impact on a Cu surface was measured. The observed line positions demonstrate electron capture into high-n states and a fast radiative decay in the neutralization process at the surface.

INTRODUCTION

An electron-beam ion trap (EBIT) has recently been developed for studying interactions of fast electrons with highly charged high-Z ions.[1,2] It has successfully been applied for studies of dielectronic recombination and for high-resolution x-ray spectroscopy.[3] Ionic charge states up to 82+ in uranium have been produced in the trap and the dielectronic recombination has been measured for various ions. The ionization, recombination, or excitation of ions in the trap is achieved by injecting an electron beam with appropriate energy and density in a manner similar to that used in an electron-beam ion source[4,5] (EBIS). The electron beam serves two purposes. It ionizes or excites the ions and it traps the ions radially. Longitudinal trapping of the ions is done by a potential well.[1,2] Previously, the ions and their ionization state were detected by observing the x-ray emission from side ports in the trap. Therefore ions produced in excited states which stabilize by emitting x rays were seen. The EBIT in the "trapping mode" is therefore suitable for measuring dielectronic recombination (DR) and electron-impact-excitation cross sections.[1,2] In order to measure, e.g., dielectronic recombination, the electron beam first produces the initial ion charge states. The electron-beam energy is then scanned through the dielectronic recombination resonance energies, whereby recombination radiation is observed as a function of the electron-beam energy.

In order to measure directly the charge-state distribution of ions in the trap and in order to obtain cross sections for ionization and excitation in comparison with cross sections obtained from x-ray measurements, as well as DR cross sections, which lead to a change of the ionic charge but not necessarily to x-ray emission, the ions have to be extracted for charge analysis. Different modes of extracting the ions from the EBIT can be applied such as continuous or pulsed extraction. In the continuous extraction mode, ions that have obtained enough energy by collisional heating through electron-impact and ion-ion collisions escape longitudinally from the trapping potential. In the pulsed extraction mode the trap is emptied instantaneously and all the ions in the trap can be detected. Then trapping time dependences up to the equilibrium charge-state distributions can also be studied. The charge-state distributions reveal final charge states in the sense that nonradiative (autoionizing) decay has already occurred in the trap. Only small fractions of metastable components are expected to effect the final charge-state distribution. We have investigated both schemes of ion extraction from the EBIT. The purpose of the experiments was to demonstrate the feasibility of this method for obtaining ion charge-state distributions independently from x-ray measurements in the trap. We have demonstrated that the extracted ions can be used as a beam of slow, very highly charged ions for atomic-collision experiments and we have shown that ion surface interaction studies can be performed. Future experiments will include the measurement of ion cooling properties, e.g., in the energy distribution of the ions ejected from the trap, energy gain spectroscopy, or retrapping of ions for experiments with laser and possibly synchrotron radiation.

EXPERIMENT

The ion trap has been described in detail in Refs. 1 and 2. A schematic of the EBIT including the ion extraction and analyzing system is shown in Fig. 1. The actual trap volume consists of a copper cylinder (drift tube) with an inside diameter of 10 mm over a length of 43 mm. An additional drift tube at each end of the trap volume is biased to provide axial ion confinement. The electrons are produced from a Pierce gun and injected axially into a magnetic field produced by superconducting Helmholtz coils. The electron beam is compressed adiabatically when entering the field, causing electron densities of about 2000 A/cm^2 at beam currents around 100 mA. The electron-beam radius is then maintained at about 35

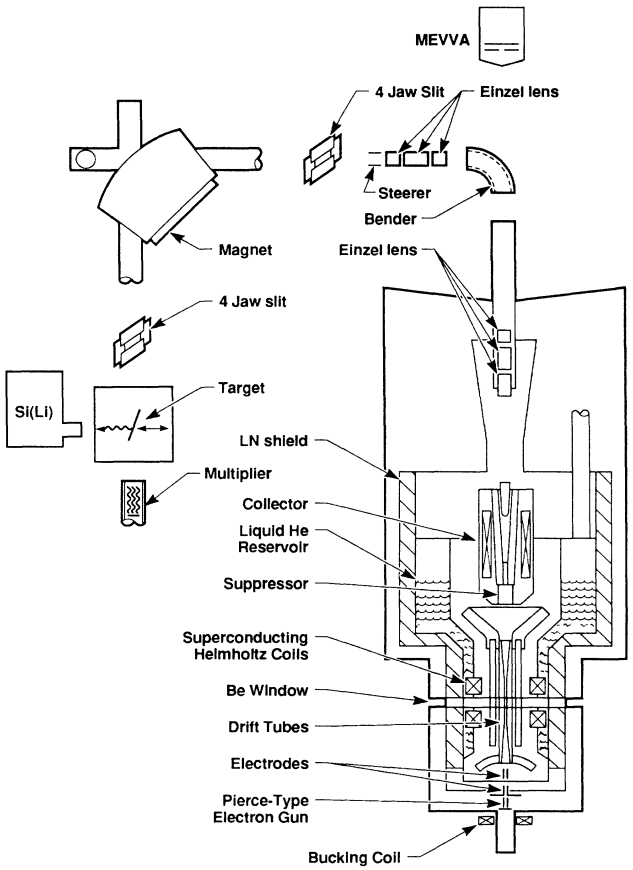

FIG. 1. Schematic of the extraction system attached to EBIT including the Cu target arrangement of the MEVVA (metal vapor vacuum arc) ion source.

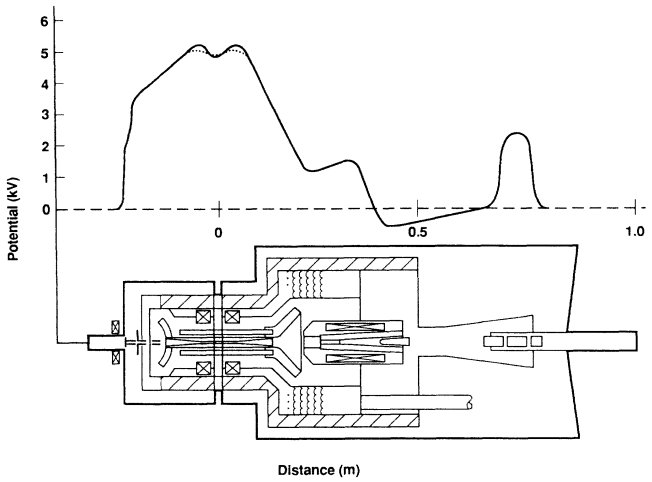

FIG. 2. Schematic of the electric potentials along the EBIT axis ranging from the electron gun anode to the einzel lens (5-kV extraction potential on the trap). The dashed line indicates the possibility to adjust the potential well on the trap.

μm in a magnetic holding field of 3 T. The potential due to the electron-beam space charge does reduce the beam energy by typically about 170 V in the 10-mm-diam trap part and by about 130 V at the narrower drift tube ends. This potential difference (40 V) traps the ions axially; a trapping voltage of about 15 V between the beam center and the drift tube wall trap the ions radially. The various measurements of the dielectronic recombination[2] have shown that the energy spread in the electron beam is about 50 eV [full width at half-maximum (FWHM)]. The drift tubes, trapping cylinder, and Helmholtz coils are operated at liquid He temperatures (4 K).

Ar or Xe gas was injected through one of the side ports into the trap. The gas atoms are then ionized and excited successively by the electron beam in the trap. The important condition for a most efficient electron-impact ionization and excitation is a maximum overalp between the electron beam and the trapped ions. Different channels for electron-impact ionization, excitation, and recombination can then be studied as a function of electron-beam energy. For the first experiments the electron-beam energy was varied between 2 and 10 keV, producing charge states for Ar from 7+ up to and including 18+ and for Xe between about 8+ and 48+. A positive potential of 8 kV on the trap (see radial potential curve in Fig. 2) for example causes ions to be expelled with energies of (8 kV)$\times n$ (n being the ion charge state) towards the first element of the einzel lens at ground potential.

Both the einzel lens and the extractor (negative bias) serve as focusing elements on the extracted ions as they approach the electrostatic bender. The electrostatic bender is followed by an einzel lens, a set of xy steering plates and a 90° analyzing magnet. The magnetic field (maximum 5 kG) is used to charge, mass, and momentum analyze the extracted ions. The slits ("4 jaw") before and after the magnet are used to determine the momentum resolution ($\Delta p/p \sim 0.1\%$ FWHM) and to reduce the background. The ions were detected by an open multiplier with a detection efficiency of about 60%. It should be noted that the electron beam focuses and guides the ions to some extent up to the electron collector. The ion beam has an emittance of about 1 cm rad keV$^{1/2}$.

In the continuous extraction mode, ions drift continuously out of the trap after having been trapped for some short time interval (~ 1 ms). This trapping time is sufficient to produce highly ionized ion configurations. The ions gain energy ("heating") mainly from electron-ion collisions and overcome the drift-tube potential. The potential well of the trap can be varied by either changing the potential (50–200 V) on the drift-tube ends or the trap potential (dotted curve in Fig. 2). This is done by a bias floating atop of the high voltage extraction potential. It should be noted that if the well is varied by an additional floating potential on the trap, this also moderates the electron-beam energy slightly. The floating bias on the trap is also used to extract ions in the pulsed mode. There the additional bias (e.g., -200 V) on the trap is ramped to a potential just above the top drift tube. The frequency of the ramped pulse determines a confinement time which is typically 200–400 ms. The width of the extraction pulse is about 20 ms. The adjustable well potential and timing allows for an optimization of specific charge states. In general, it was found that the average emission rate, in the pulsed mode, of the higher charge

states increases by an order of magnitude as compared to the continuous extraction mode. The extracted ions are deflected out of the trap axis by 90° at about 1 m above the trap by applying an appropriate electrostatic field on the 90° cylindrical bender (Fig. 1). The bender consists of an inner (4-cm radius) and outer (6-cm radius) cylindrical segment. These segments consist of high transmission gold grids. This particular setup allows ions to be axially injected and focused via the einzel lens into the EBIT from an ion source [MEVVA (metal vapor vacuum arc) in Fig. 1] above the electrostatic bender. The injection mode with the MEVVA has successfully been used to produce and extract high rates ($\sim 10^4$ per pulse) of highly charged thorium and uranium ions up to Th and U at 24- and 9-keV electron-beam energies [Figs. 3(a) and 3(b)], respectively; these results will be discussed in a forthcoming publication.

The extraction potential also defines the electron-beam energy. Charge-state distributions as a function of the electron-beam energy between 2 and 10 keV have been measured in the continuous mode. There the electron-beam current was kept at a fixed value around 100 mA during the scans and the spectra were normalized to a constant time interval for data accumulation at each data point. The reproducibility of the spectra was tested and appears to be within ±10%.

For measuring x rays emitted in the neutralization process of highly charged Ar and Xe ions on solid surfaces, a copper target was inserted in front of the multiplier and viewed by a Si(Li) detector. The geometrical solid angle of this detector was 3×10^{-3} sr and its resolution was 200 eV at 5.9 keV. The detector was separated from the chamber vacuum by Be foils of a total 75 mm thickness. For the Ar $K\alpha$ and Xe $L\alpha$ x-ray lines at about 3.3 and 4.5 keV, respectively, the absorption is negligibly small.

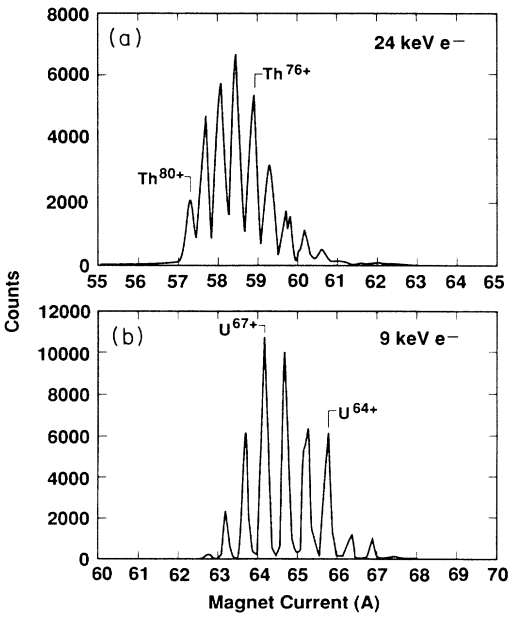

FIG. 3. Spectrum of charged analyzed (a) thorium and (b) uranium ions following 9-keV electron impact.

The vacuum in the beam transport system between the EBIT and the magnet was on the order of 10^{-9} Torr and the charge change by capture is estimated to be negligible. Between the magnet and the Cu target the vacuum was on the order of 10^{-8} Torr; from this we estimate a loss of ions with inner-shell vacancies of less than 10%. The detected characteristic x-ray intensity can therefore provide a measure for the number of ions with inner-shell vacancies emerging from the EBIT.

RESULTS AND DISCUSSION

Figure 4 displays charge-state distributions of extracted Ar ions in the (a) pulsed and (b) continuous (leaky) modes using a 9-kV extraction potentials on the trap. The different peaks in the spectra are labeled according to the different ion charge states. Also labeled are peaks that result from ions due to background gas excitation in the trap. The background contaminants appear to be mainly $O^{8+,7+,4+}$, $N^{7+,5+,3+}$, and $C^{6+,4+}$, which serve also as calibration lines for the spectra.

The dashed line indicates a charge-state distribution for the leaky mode obtained from a modeling calculation solving essentially rate equations with relevant electron-impact-ionization and recombination cross sections.[6] The agreement between the calculated and measured charge-state distribution is rather good. A rate of neutral Ar ($\sim 10^8$ atoms/cm^3 s) going into the trap was used in the calculation.

In Fig. 5 the electron-beam energy dependence of the Ar^{16+} intensities, which are normalized to the O^{8+} intensity in the spectrum, is plotted. The dependence shows a maximum at 2.25 keV. The rates for continuous extraction that have been observed for Ar ion charge states around 12+ at 3 keV beam energy are a few times 10^5 s^{-1} and about 10^4 s^{-1} for Ar^{16+}. The Ar^{17+} and Ar^{18+} charge state starts to appear at about 6 keV and a rate of about 10^4 s^{-1} was found at 9-keV electron-beam energy in the leaky mode and up to 10^5 s^{-1} in the pulsed mode ($\sim$500-ms confinement time). The L-shell binding energies for neutral Ar vary between 150 and 300 eV and the L-shell ionization maximizes at about 1-keV electron energy. Thus the drastic increase of the L-shell binding energies with a high degree of multiple ionization might explain the Ar^{16+} maximum for continuous extraction at about 2–3-keV electron-beam energy: Neutral Ar atoms that diffuse in the trap are instantaneously multiply ionized by successive electron impact. Thus a distribution of highly charged ions with increased L-shell binding energies up to about 900 eV (e.g., $2s$ in Ar^{15+}) "constantly" exists in the trap. The L shell of Ar ions around 16+ is most efficiently ionized at above 2-keV electron-beam energy (Fig. 5). As the electron-beam increases the higher charge states become more dominant. Ions with charge states 15+ through about 18+ are less effectively extracted in the continuous mode than in the pulsed mode of extraction. The average rate for Ar^{18+} and Ar^{17+} ions could be enhanced up to about an order of magnitude by tuning the confinement time and well potential; this implies a rate of ions in the extraction pulse of at least about 10^6. Since the signal from the ion detector was gated

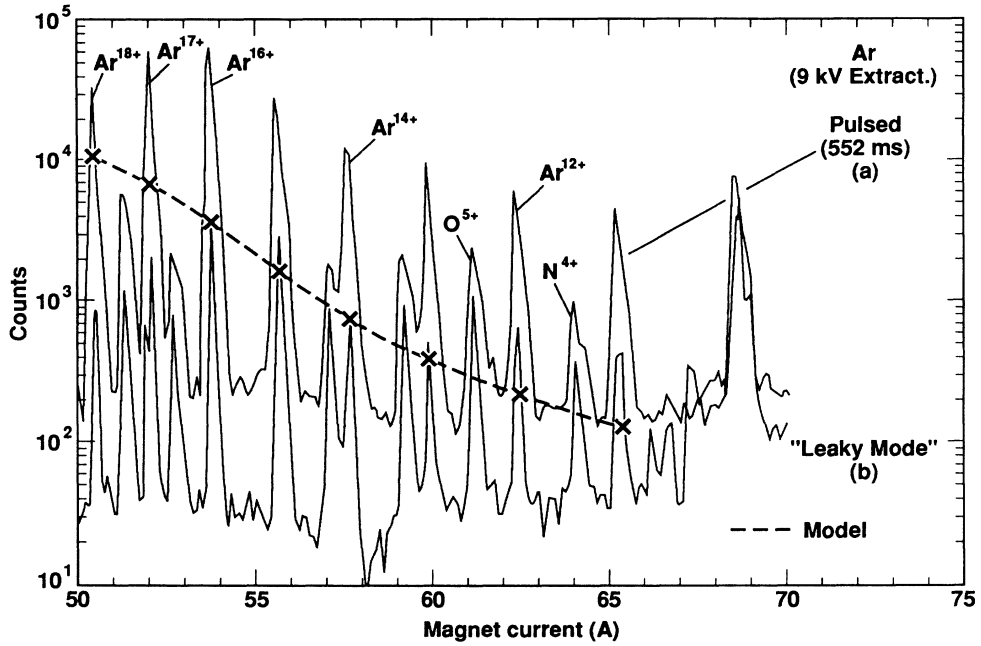

FIG. 4. Spectra of charged analyzed Ar ions for 9-kV extraction voltage; the intensities are plotted versus magnet current. Spectrum (a) is measured in a pulsed mode, spectrum (b) is measured in a continuous mode. The dashed line shows the result of modeling calculation (see Ref. 6).

with the extraction pulse, intensity due to light contaminants was reduced considerably. Specific charge states can be enhanced via DR at the corresponding electron-beam resonance energies. These resonances, which have been observed between 2- and 3.5-keV electron-beam energies for Ar can effectively be studied in a pulsed mode[7,8] by charge-state analysis or as mentioned above by measuring the characteristic x-ray emission as a function of electron-beam energy (e.g., see Ref. 2).

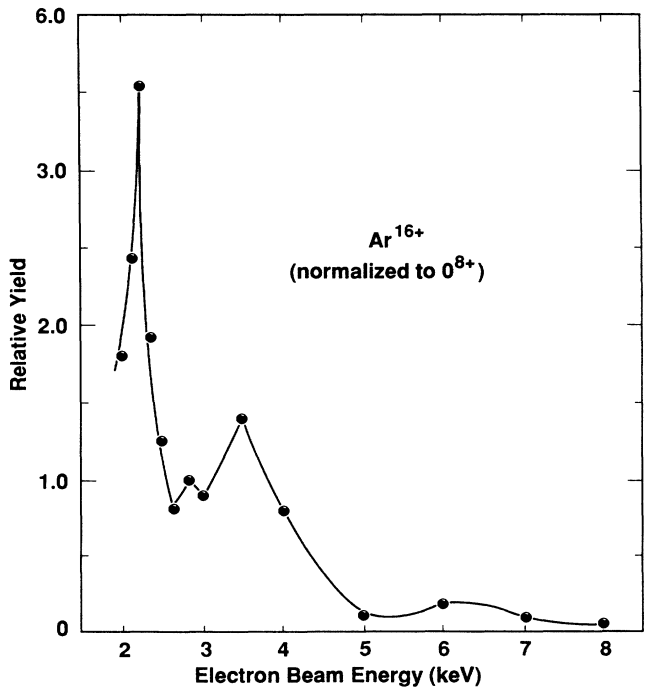

FIG. 5. Integrated intensities of charge analyzed Ar^{16+} ions vs electron-beam energies; the intensities are normalized to O^{8+}.

Ar^{17+} and Ar^{18+} ions produced in the trap with 8-keV electron impact have been used to bombard a solid Cu surface oriented at 45° relative to the ion-beam axis. The consequent Ar K x-ray emission following the decay of He- and H-like excited Ar ions was observed with a Si(Li) detector arranged perpendicular to the in-beam axis; the observed x-ray spectra are displayed in Fig. 6. The observed Ar K x-ray emission not only confirms the charge state of the extracted Ar but it also allows us to estimate the number of ions extracted in the pulsed mode. The number of ions (average rate) of $N \sim 10^4\ s^{-1}$ was found to be in agreement with the directly measured rate of the charge analyzed Ar^{18+} ions. The K x-ray spectrum from Ar^{17+} impact consists of the dominant intensity due to the shifted $K\alpha$ x-ray emission ($2p \rightarrow 1s$) at 3020 eV and that due to shifted $K\beta$ x-ray emission ($3p \rightarrow 1s$) and intensity due to $np \rightarrow 1s$ transitions. The observed energy shifts with respect to the $K\alpha$ line of an Ar atom with one K vacancy are about 70 eV for the ($2p$-$1s$) component and about 220 eV for the ($3p$-$1s$) component with respect to the $K\beta$ line of the Ar atom. The $K\alpha$ and $K\beta$ lines are shifted due to multiple L- and M-shell vacancies, consistent with earlier reported results by Donets *et al.*[4] who used slow ions (17-keV Ar^{17+}). The K x-ray peak positions agree with $K\alpha$ and $K\beta$ lines for Ar atoms carrying one K, several L, and several M holes. This confirms the picture of a "hollow" atom. That is, electron capture into the empty n levels of the ion from the surface occurs resonantly up to neutralization when the ion approaches

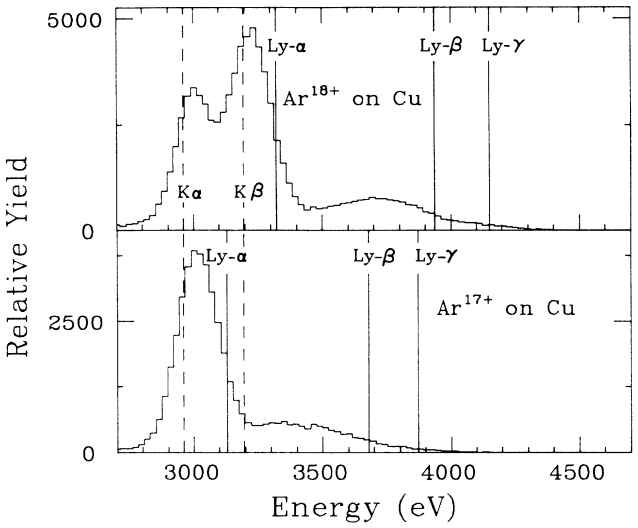

FIG. 6. Ar K x-ray spectrum following 136-keV Ar^{17+} and 144-keV Ar^{18+} ion impact on a Cu surface (45°). The spectra consist of $K\alpha$ and $K\beta$ satellite and $K\alpha^H$ and $K\beta^H$ hypersatellite x-ray emission lines. Energies for the Lyman series of He-like Ar^{16+} and H-like Ar^{17+} are from Ref. 9.

the surface. The transition into the 1s state occurs before these electrons relax to an intermediate bound state.[10] Due to the high K-shell fluorescence yield the $np \rightarrow 1s$ transitions are observed efficiently.

In Fig. 6(b), a spectrum produced with 180-keV Ar^{18+} is shown. The spectrum shows a low energy peak that matches the one for the Ar^{17+} case. It shows a second more intense peak which results from $K\alpha^H$ hypersatellite line intensities. The $K\alpha^H$ hypersatellite line intensity is enhanced by about 30% over that of the $K\alpha$ satellite line intensity. Following the electron capture into high-n levels ($n > 20$) radiative and Auger decay fill one vacancy, thus one observed x-ray emission from ions with one or two initial K vacancies. The comparable intensities reflect the similar mean K-shell fluorescence yield for single and double K-vacancy ions with partly filled L and M shells; the mean K-shell fluorescence yield for such a case is about 15%.[11] A more detailed analysis requires extended calculations for decay rates and transition energies. The third peak is a shifted broader structure and results mainly from $K\beta$ satellite and hypersatellite line intensities.

Figures 7(a) and 7(b) shows charge-state distributions [(a) pulsed mode and (b) continuous mode] obtained for the case where ^{136}Xe gas is diffused into the trap. The isotope ^{136}Xe has been used in order to avoid overlap of charge-state contributions from different isotopes; some intensity from the ^{134}Xe isotope is visible. The distributions were measured for different electron-beam energies (trap extraction potentials) which are not all shown here. Again the centroid of the charge-state distribution changes drastically with the electron-beam energy and charge states ranging from Xe^{12+} to Xe^{45+} are observed. At about 5.5 keV, for example, the charge-state distribution peaks around Xe^{18+}. The rates of Xe^{44+}, for example, were about $10^4\ s^{-1}$ while rates up to $10^5\ s^{-1}$ were observed for Xe^{37+} ions.

Figure 7(a) shows a charge-state distribution following the ion extraction in a pulsed mode. The average intensity is again, as in the case of Ar, increased by a factor of 10 and here higher charge states up to 48+ are observed. It is also noted that contributions due to residual gas ionization are suppressed in the pulsed mode.

The integrated peak intensity from spectra measured in the leaky mode as a function of electron-beam energies are plotted versus the electron-beam energy in Fig. 8 where the Xe^{44+} intensity is normalized to the C^{4+} intensity. Similar to the Ar case, a sharp rise in the intensity from about 4.5 keV is observed.

The measurements are in qualitative agreement with calculated electron-impact ionization cross sections for Xe^{43+}. The calculated cross sections are shown in Fig. 8. The dashed line is the cross section for direct ionization of the 3s electron. For beam energies above 4 keV it is possible to excite 2p electrons to the $n = 3$ levels and produce autoionizing states of the ion. Near the thresholds for these excitations the ionization cross section increases abruptly due to these excitation-autoionization contributions to the cross section. Some of these excitations can decay radiatively rather than by autoionization. To ob-

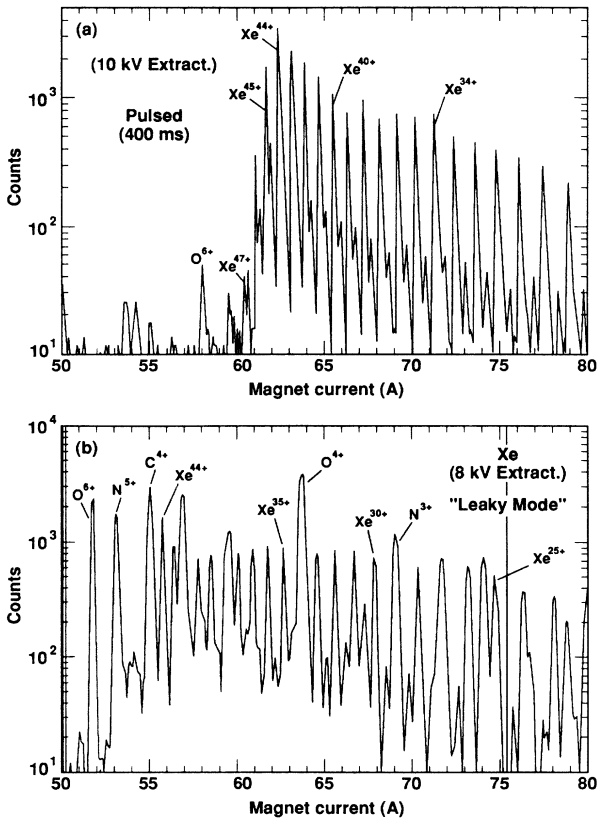

FIG. 7. Spectra of charge analyzed $^{136}Xe^{N+}$ ions for different electron-beam energies. Spectrum in (a) is measured in pulsed mode, an abundance of 10% from ^{134}Xe is observed in the spectra; spectrum in (b) is measured in a continuum mode.

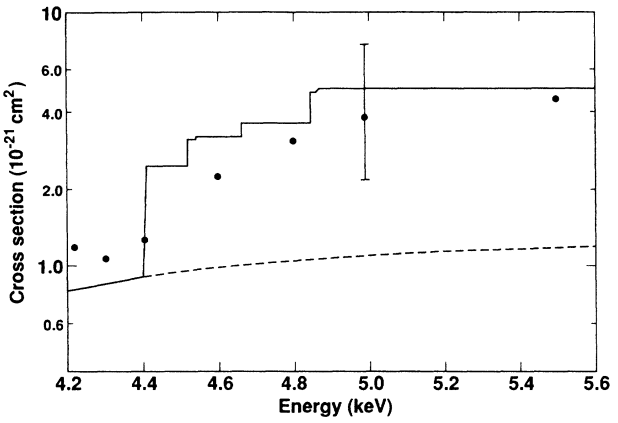

FIG. 8. Integrated intensities of charge analyzed Xe ions (44+) vs electron-beam energies; the intensities are normalized to C^{4+}. The experimental data (solid circles) are compared to calculated electron-impact-ionization cross sections. The dashed line is the cross section for the direct ionization of the 3*s* electron. The solid line is the sum of the direct and excitation-autoionization cross sections with radiative decay taken into account.

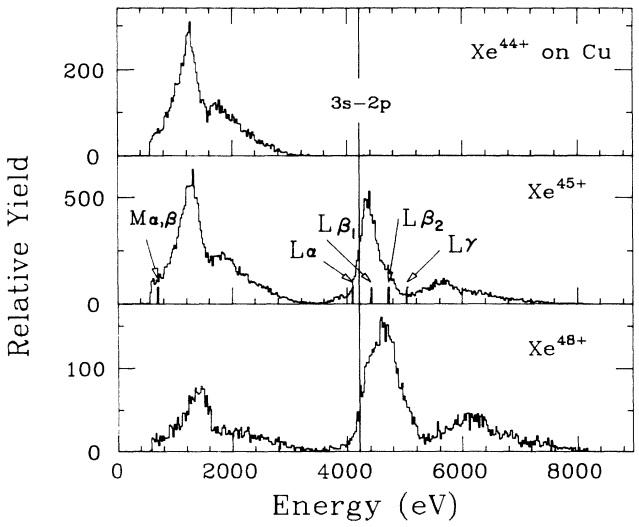

FIG. 9. Xe *M* and *L* x-ray emission spectra obtained from Xe^{44+}, Xe^{45+}, and Xe^{48+} ion impact on a Cu surface (45°).

tain the correct ionization cross section, each excitation cross section is multiplied by a branching ratio and then added to the direct ionization cross section. The solid curve in Fig. 8 shows the effects of excitation-autoionization with radiation taken into account, and this curve is compared with experimental results. The theoretical results shown in Fig. 8 are discussed in detail elsewhere.[12] The ionization cross section increases by a factor of 4 in a series of abrupt steps between 4 and 5 keV. Since ionization transforms Xe^{43+} to Xe^{44+}, this increase in the cross section should be manifested by a similar increase in the ratio of Xe^{44+} to Xe^{43+} ions in the trap. Although the resolution is not sufficient to show any step structure in detail, the experimental data show a large increase in the ratio of Xe^{44+} to Xe^{43+} in this region as the theory predicts.

Figures 9(a)–9(c) show Xe, *M*, and *L* x-ray spectra from Xe^{44+}, Xe^{45+}, and Xe^{48+} ion impact on Cu. The Xe^{44+} spectrum consist of the *M* x-ray spectrum alone since there is no *L* vacancy in the ion. Xe^{45+} and Xe^{48+} spectra show in addition intensities from *L* x rays. Recently reported line energies for the neonlike doublet in $Xe(2p^5_{3/2}3s_{1/2})_{J=1,2}\rightarrow 2p^6$ are plotted for comparison.[13] The spectra show an energy shift towards higher energies with increasing charge states in the *L* x-ray spectra due to the increasing number of *L* vacancies. For the Xe^{45+} the *M* x-ray intensity is somewhat shifted towards higher x-ray intensities indicating the inner-shell vacancies. The spectrum shows $L\alpha$ and $L\beta$ x-ray intensity due to the initially existing *L*-shell vacancy. The shift of the $M\alpha$ and $M\beta$ x rays with respect to the neutral atom $M\alpha$ x-ray emission is about 400 and 600 eV, respectively. The energy shift of the observed *L* x-ray emission is about 200 eV with regard to the neutral atom *L* x-rays. For the Xe^{48+}, the observed *M* and *L* x-ray intensities are shifted again toward higher x-ray energies reflecting the increased number of inner- and outer-shell vacancies. The observed x-ray emission infers qualitatively the picture that a hollow atom configuration for Xe^{48+} is formed as the ion interacts with the Cu surface. Furthermore, it appears that the relative intensities between *M* and *L* x-rays are changing with increasing charge states. The increase in the *L* x-ray intensity relative to the *M* x rays is due to an increase of the fluorescence yield with an increasing number of *L* vacancies. For the Xe^{48+} case we observed an increased width in the *L* x-ray emission peak if compared to the Se^{45+} case which is due to the increased number of *L* vacancies. This is similar to comparison of the Ar^{17+} and Ar^{18+} case for the *U* x-ray emission. These preliminary results will be subject of further theoretical and experimental investigations.

CONCLUSION

Results for the extraction of highly ionized Ar and Xe ions following electron-impact and excitation in an electron-beam ion trap are reported. For Ar ions, charge states up to 18+ have been extracted, for Xe ionic charges up to 48+ have efficiently been produced and are extracted from the trap. The ions were extracted in a continuous and pulsed mode and rates between 10^3 s and 10^5 s^{-1} are observed for individual charge states. In the case of Ar, 17- and 18-times charged ions were extracted and impinged on a solid Cu surface. Characteristic Ar *K* x-ray emission has been observed indicating the population of high-*n* states in core excited H- and He-like Ar ions. For $Xe^{44+,45+,48+}$ *L* x-ray emission has been observed following the ion impact on solid surfaces. This paper demonstrates the extension of the capabilities of an electron-beam ion trap through the application of an efficient ion extraction system to study the physics of highly charged high-*Z* ions in collisions.

ACKNOWLEDGMENTS

The valuable technical support by D. Nelson and E. McGee in the performance of these experiments is greatly acknowledged. This work was performed under the auspices of the U.S. Department of Energy by the Lawrence Livermore National Laboratory under Contract No. W-7405-ENG-48.

---

*Also at Manne Siegbahn Institute, Stockholm, Sweden.
†Also at Kansas State University, Manhattan, KS.
‡Also at Sandia Laboratories, Livermore, CA.

[1]M. A. Levine, R. E. Marrs, J. R. Henderson, D. A. Knapp, and M. B. Schneider, Phys. Scr. **T22**, 157 (1988); M. A. Levine, Nucl. Instrum. Methods B **43**, 431 (1989).

[2]R. E. Marrs, M. A. Levine, D. A. Knapp, and J. R. Henderson, Phys. Rev. Lett. **60**, 1715 (1988).

[3]P. Beiersdorfer, in *X-Ray and Inner-Shell Processes, Knoxville, 1990,* Proceedings of the Conference on X-Ray and Inner-Shell Processes, AIP Conf. Proc. No. 215, edited by Manfred Krause and Thomas Carlson (AIP, New York, 1990).

[4]E. D. Donets, Nucl. Instrum. Methods B **9**, 522 (1985); E. D. Donets, IEEE Trans. Nucl. Sci. **NS-23**, 897 (1976).

[5]P. A. Redhead, Can. J. Phys. **45**, 1791 (1967).

[6]B. Penetrante *et al.* (unpublished).

[7]D. A. Knapp, R. E. Marrs, M. A. Levine, C. L. Bennett, M. H. Chen, J. R. Henderson, M. B. Schneider, and J. H. Scofield, Phys. Rev. Lett. **62**, 2104 (1990).

[8]R. Ali, C. P. Bhalla, C. L. Cocke, and M. Stockli, Phys. Rev. Lett. **64**, 633 (1990); D. De Witt (unpublished).

[9]J. H. Scofield (private communication).

[10]J. Andrä, Nucl. Instrum. Methods B **43**, 3 (1989); **43**, 306 (1989).

[11]K. Karim and C. P. Bhalla, Phys. Scr. **38**, 795 (1988).

[12]K. J. Reed, M. H. Chen, and D. H. Moores, Phys. Rev. A (to be published).

[13]P. Beiersdorfer, S. von Goeler, M. Bitter, E. Hinnov, R. Bell, S. Bernabei, J. Felt, K. W. Hill, R. Hulse, J. Stevens, S. Suckewer, J. Timberlake, A. Wouters, M. H. Chen, J. H. Scofield, D. D. Dietrich, M. Gerassimenko, E. Silver, R. S. Walling, and P. L. Hagelstein, Phys. Rev. A **37**, 11 (1988); **37**, 4153 (1988).